Effect of TiO_2 and synthesis strategies on formate oxidation: Electrochemical and Fuel Cell approaches

Vitória Pistori Guimarães[1]; Júlio Nandenha[2]; Luiz Otávio Orzari[3, 4]; Orlando Fatibello-Filho[5]; Almir Oliveira Neto[2]; Bruno Campos Janegitz[3]; Fernando Campanhã Vicentini[1]; Mônica Helena Marcon Teixeira Assumpção[1]*

[1]Federal University of São Carlos (UFSCar), Lagoa do Sino *Campus*, 18290-000, Buri, SP, Brazil

[2]Nuclear and Energy Research Institute (IPEN/CNEN), University City, 05508-000, São Paulo, SP, Brazil

[3]Federal University of São Carlos, Department of Nature Sciences, Mathematics and Education, 13600-970, Araras, SP, Brazil

[4]Department of Physics, Chemistry, and Mathematics, Federal University of São Carlos, 18052-780, Sorocaba, SP, Brazil

[5]Federal University of São Carlos (UFSCar), Department of Chemistry, 13560-970, São Carlos, SP, Brazil

* Corresponding author: Tel.: +55-15-3256-9064;

e-mail: monicahelena@ufscar.br (Mônica Helena Marcon Teixeira Assumpção)

(The authors declared that they have no conflict of interest)

Abstract

Direct Formate Fuel Cells have gained increasing attention since formate can be obtained by CO_2 reduction, being shown as a renewable power source. This paper reports the use of Pd nanoparticles supported on physical mixtures of Vulcan carbon and TiO_2 in different ratios and different Pd reduction methodologies. The materials were prepared using sodium borohydride as a reducing agent and analyzed toward formate oxidation in alkaline media. The prepared electrocatalysts showed peaks of Pd face-centered cubic and TiO_2 anatase and rutile phases and an average particle size between 3.7 and 7.9 nm. Experiments considering formate electro-oxidation (voltammetry and chronoamperometry) showed that the presence of TiO_2 is favorably using both synthesis methodologies while single-cells revealed Pd nanoparticles supported on physical mixtures of carbon and TiO_2, in the proportion of (75:25) as the most efficient, which was explained by the carbon high electrical conductivity and small quantities of TiO_2 working as co-catalyst.

Keywords: Pd nanoparticles; TiO_2; formate electro-oxidation; Direct Formate Fuel Cell.

1. Introduction

According to Goldemberg [1] the marvelous machine produced by the evolutionary process – the human body – is driven by water, oxygen, and by food which supplies the modest energy needed for a human to go around and produce knowledge likewise the machines that drive our modern society. However, these machines consume huge amounts of energy. As stated by International Energy Agency (IEA), the energy consumption of the world economy increased around twice from 1975 to 2015 [2] and estimations reveal that energy utilization will increase by around 30% between 2015 and 2040, worldwide [3].

Most energy consumption comes from fossil fuels such as coal, oil, and natural gas. About 80% of the energy consumed in the world is supplied by this type of fuel, which is worrying since it has been recognized that human civilization is over-exploiting the planet´s resources faster than they are being renewed [4-6]. Additionally, although fossil fuels are still the cheapest energy source, it is non-renewable and reserves will deplete and run out, eventually. Moreover, burning this energy source increases CO_2 emissions, and consequently contributes to climate change, which emerged as a major concern for humanity over the last two decades [7, 8].

With this scenario, the power industry seeks to increase the production of renewable energy production to meet energy demands with more sustainable development [5]. In this context, many effective approaches can be used to reduce the influence of CO_2 emissions and an example is the fuel cell, an electrochemical device that combines chemical fuels and electrocatalysts to produce electricity cleanly [6, 9].

Among the fuel cell types, the Direct Liquid Fuel Cell (DLFC) is under intense study due to its advantages over hydrogen-based ones, which need to store the explosive

fuel under high pressure, while also being flammable and presenting transportation issues, besides, it shows simple structural design [10-14]. In DLFC, the liquid fuel is oxidized at the anode, and the oxygen gas is reduced at the cathode. The charged ions pass through the electrolyte and the electrons travel through an external circuit. Many liquid fuels have been used in DLFC, but alcohols (such as ethanol and methanol) are the most common [10, 14].

However, formate has been emerging as a promising fuel since it is non-flammable, non-toxic, relatively low cost, and renewable, as it can be obtained from the electrochemical reduction of CO_2 [15, 16]. Thus, formate also gives a lower theoretical reversible potential (Equation 1) which combined with the cathode half-reaction (Equation 2) results in an overall theoretical voltage for the direct formate fuel cell of 1.45 V, a value of 0.24 V and 0.31 V higher than those cells using methanol and ethanol as fuel, respectively [17, 18].

$$HCOO^- + 3\ OH^- \rightarrow CO_3^{2-} + 2\ H_2O + 2e^- \ (E^0 = -1.05\ V) \quad (1)$$

$$\tfrac{1}{2}\ O_2 + H_2O + 2e^- \rightarrow 2\ OH^- \ (E^0 = 0.40\ V) \quad (2)$$

One drawback faced by DLFC is the high cost of electrocatalysts [14, 19, 20]. As reported by An et al, formate oxidation is facile in alkaline media using palladium electrocatalysts [21], however, it is a most costly material, which hinders the development of fuel cells [22]. Thus, one way to improve the catalyst utilization and decrease the fuel cell cost is by using nanoparticles supported by carbon materials due to their high electrical conductivity. However, carbon is susceptible to corrosion which makes it less favorable for fuel cell applications, therefore, its replacement by a metallic oxide could be extremely important [23, 24].

According to Bandarenka et al [25], one common factor that controls catalyst performance is the interaction between nanoparticles and supports. Hence, another way

to improve the electrocatalysts' efficiency is by developing different supporting materials [10, 26]. Among them, TiO_2 shows good mechanical resistance and stability in oxidative environments, it is non-toxic, and has a relatively low price, characteristics that suggest TiO_2 as alternative support. Furthermore, TiO_2 could show the co-catalytic effect on fuel oxidation [23, 27-29], which is an advantage since according to the Sabatier principle [25, 30], the surface of the active electrocatalyst should be able to activate the reactants and at the same time should not bind the reaction intermediates too strongly to prevent poisoning of the active site.

Considering the use of TiO_2 as a support, it is also important to highlight that theoretical studies showed that spontaneous dissociative H_2O adsorption occurs on the (001) TiO_2 surface, whereas molecular H_2O adsorption is prevalent on the (101) surface. The crystallite shape of anatase (phase of titanium oxide) is a truncated bipyramid, exposing both the (101) and (001) surfaces, then a large quantity of (001) surface planes can be supplied by TiO_2. So, dissociative H_2O adsorption on the (001) anatase surface produces a plentiful Ti-OH surface group, improving the bifunctional mechanism [24, 31].

Although TiO_2 shows low electrical conductivity and surface area [32], when compared to carbon black it could act as a co-catalyst and also improve the bifunctional mechanism. In this context, in this work, we studied the efficiency of Pd nanoparticles supported on physical mixtures of carbon black and TiO_2, toward formate oxidation, in alkaline media. We also investigated the influence of the TiO_2 introduction in the catalysts by using different synthesis methodologies. In the first one, the Pd was reduced in a physical mixture of carbon and TiO_2, and in the second one, the Pd was reduced firstly in TiO_2, and carbon was inserted after this step. All the prepared electrocatalysts were studied considering not only the electrochemical but also the fuel cell experiments. To

120 the best of our knowledge, this is the first time that the oxidation of formate is studied
121 using Pd on different supports of carbon and TiO_2, regarding also the synthesis strategies.
122
123 **2. Experimental**
124
125 2.1. Synthesis of the catalysts
126 Pd nanoparticles (PdNP) were obtained by the borohydride method [33, 34] using
127 $Pd(NO_3)_2 \cdot 2H_2O$ (Aldrich) as the metal source, Vulcan XC72 (Cabot) + TiO_2 P25
128 (Degussa) as supports, and sodium borohydride (Aldrich) as reducing agent. The
129 electrocatalysts were prepared in two batches. In the first one, the PdNP was reduced in
130 the physical mixture of carbon (C) + TiO_2, and these electrocatalysts were called
131 Pd/(C+TiO_2). In the second one, the PdNP was firstly reduced in TiO_2, and C was inserted
132 after. These electrocatalysts were called Pd/TiO_2-C. In all prepared materials the mass
133 proportions of the supports C:TiO_2 were studied in the following mass ratio percentages:
134 75:25, 50:50 and 25:75. The C:TiO_2 ratio was maintained by weighting different amounts
135 of the materials considering the total mass of support. The metal loading was set to
136 20 wt%.
137
138 2.2. Physical Characterizations
139 To study the morphology of the prepared electrocatalysts, Transmission Electron
140 Microscopy (TEM) was employed by using a JEOL-JEM-2100 electron microscope with
141 a 200 KV voltage at Instituto de Pesquisa Energéticas e Nucleares. The average size of
142 the nanoparticles was obtained using ImageJ software and the nanoparticles mean
143 diameter counting procedure was performed over 100 nanoparticles. X-ray diffraction
144 (XRD) patterns were taken by PANanalytical X´Pert PRO with CoKα radiation source

145 (λ = 0.179 nm) conducted in the range of 2θ = 20° to 110° with a step size of 0.05° and
146 scan time of 2 s per step at Laboratório Nacional de Pesquisa em Energia e Materiais
147 (CNPEM) at Campinas - Brazil. For comparison, XRD patterns were converted to CuKα
148 using Bragg law.
149
150 2.3. Electrochemical Measurements
151 Electrochemical measurements were carried out in a one-compartment glass cell
152 and three-electrode setup (half-cell): an Ag/AgCl/KCl (3.0 mol L^{-1}) was used as a
153 reference electrode; a platinum foil as a counter electrode; and the working electrode was
154 a glassy carbon electrode (Ø = 3.0 mm: geometric area of ~ 7 mm^2) used as the substrate
155 for electrocatalysts films. The catalysts were applied to de glassy carbon electrode (GCE)
156 by adding 5μL of a catalyst suspension and dried at room temperature. The catalyst
157 suspension was prepared by sonicating 6 mg of the catalyst powder, 900 μL of water,
158 100 μL of isopropyl alcohol, and 20 μL of 5% Nafion® solution.
159 Cyclic Voltammetry (CV) and Chronoamperometry (CA) analyses were
160 conducted in a potentiostat/galvanostat μStat 200 (DropSens) controlled by DropView
161 1.3 software. The CV curves were recorded at the potential limits of –0.85 V and 0.05 V
162 with a potential scan rate of 10 mV s^{-1} in 2.0 mol L^{-1} potassium hydroxide aqueous
163 solution in the presence and absence of 0.02 mol L^{-1} potassium formate. The CA curves
164 were obtained in the electrolyte composed of KOH and HCOOK at –0.55 V for 1800 s.
165 The current densities were normalized to the Pd mass.
166 The Electrochemical Impedance Spectroscopy (EIS) analyses were performed in
167 a PGSTAT204 potentiostat/galvanostat (Metrohm, Eco-Chemie), in a conventional three-
168 electrode cell, namely: GCE, Platinum, and Ag/AgCl/KCl (3.0 mol L^{-1}) respectively as
169 working, auxiliary and reference electrodes. The tests were carried out in the presence of

1.0 mmol L^{-1} $[Fe(CN_6)]^{3-/4-}$, in a 0.1 mol L^{-1} KCl medium. The technique was performed with a potential of 0.2 V ($E_{1/2}$ of the system, identified by CV) with sine type wave, amplitude of 10 mV, and frequency ranging from 10^5 to 0.1 Hz.

The dispersion with the electrocatalysts was prepared in the proportion of 12 mg to 1800 μL of ultra-pure water (resistivity ≥ 18.0 MΩ cm), 200 μL of isopropyl alcohol, and 40 μL of Nafion. The dispersion was then ultrasonicated for 30 min, and 6.0 μL was cast on the GCE surface, with a drying time of 90 min before use.

2.4. Fuel Cell Measurements

The polarization curves of a 5 cm^2 single-cell area were recorded using a PGSTAT 302N potentiostat/galvanostat Autolab. The Membrane Electrode Assemblies (MEA) were prepared as reported previously [35]. The electrocatalyst dispersion prepared using Nafion® solution (5 wt%, Aldrich) was painted over a carbon cloth. The catalytic ink was formulated in a way that Nafion® comprised 35 % wt% of the total solids in the ink and this was applied to the carbon cloth. After its preparation, the electrodes were hot-pressed on both sides of a Nafion® 117 membrane at 125 ºC for 10 min under a pressure of 247 kgf cm^{-2}. Before being used, the membranes were exposed to 6 mol L^{-1} KOH for 24 h. All cathodes and anodes were prepared with 1.0 mg metal cm^{-2} of metal loading. In all experiments, the fuel cell was maintained at 60 °C and the oxygen humidifier at 85 °C with a flow rate of 150 mL min^{-1}. The fuel, 1.0 mol L^{-1} HCOONa and 2.0 mol L^{-1} NaOH was delivered at 1.0 mL min^{-1}. A commercial Pt/C (BASF) cathode was used in all experiments.

3. Results and discussion

3.1. Physical Characterizations

Figure 1 shows the TEM images which evidence more dispersed nanoparticles on Pd/(C+TiO_2) batches when compared to Pd/TiO_2-C, although the mean particle sizes are similar. The histograms of all electrocatalysts were prepared to reveal that the mean particle sizes are in the range of 3.7 to 7.9 nm. According to Song et al. [36] the agglomeration of Pd particles can easily occur on TiO_2 supports when the Pd is loaded on TiO_2 supports, which could make the active surface area lower, reducing the catalytic efficiency.

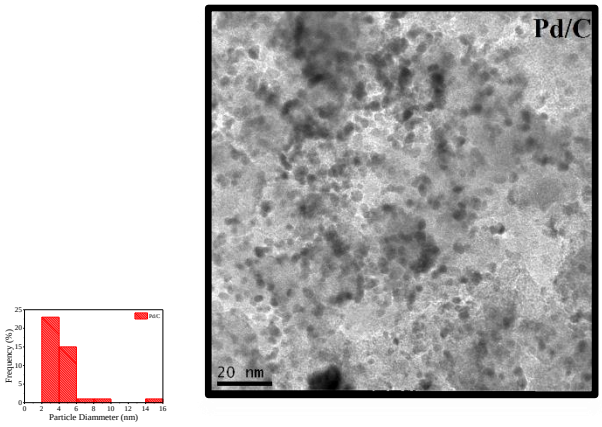

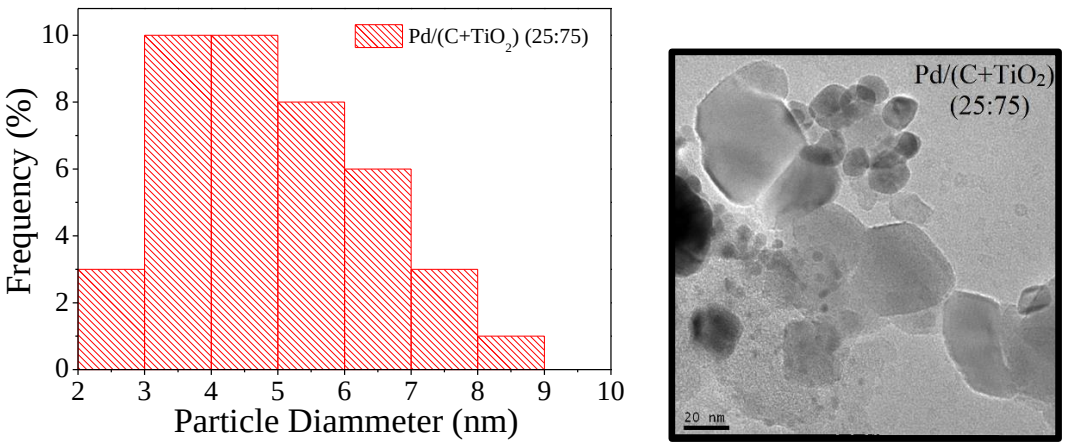

206

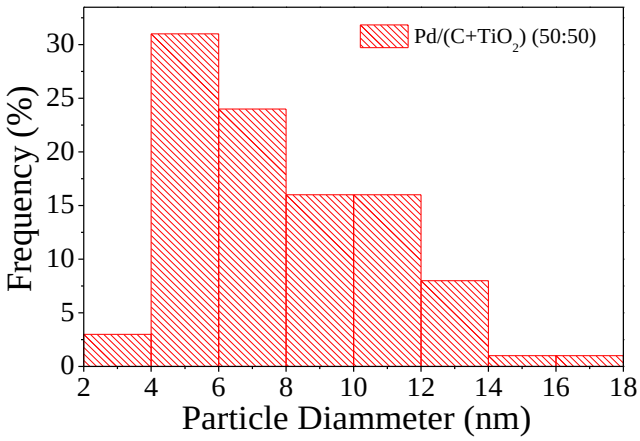
Pd/(C+TiO2) (50:50)
Frequency (%)
Particle Diammeter (nm)

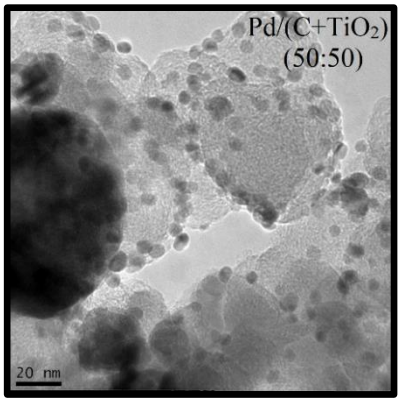
Pd/(C+TiO2)
(50:50)
20 nm

207

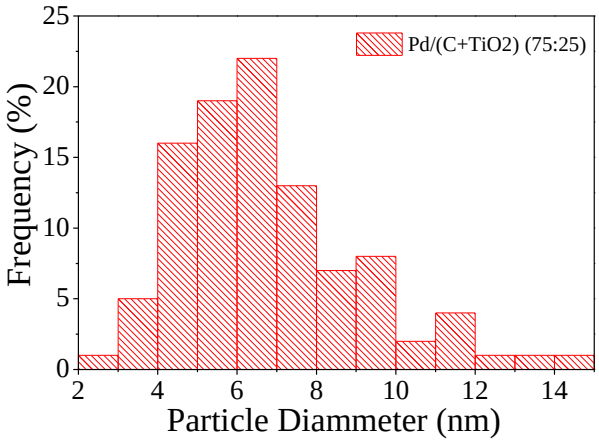
Pd/(C+TiO2) (75:25)
Frequency (%)
Particle Diammeter (nm)

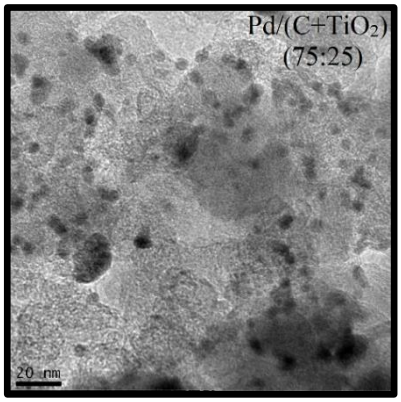
Pd/(C+TiO2)
(75:25)
20 nm

208

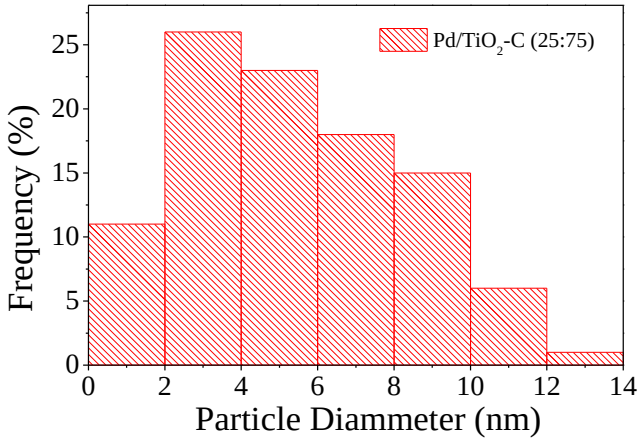
Pd/TiO2-C (25:75)
Frequency (%)
Particle Diammeter (nm)

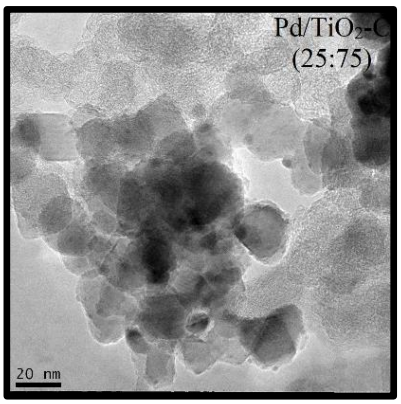
Pd/TiO2-C
(25:75)
20 nm

209

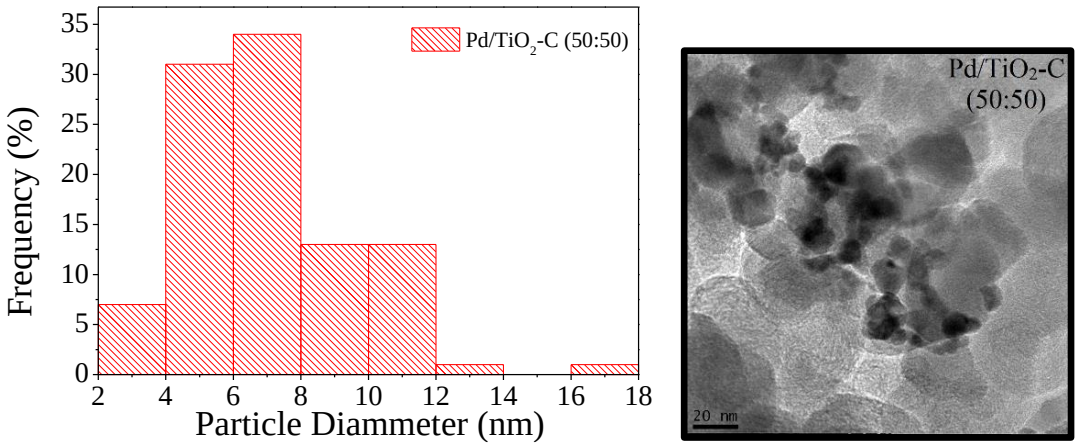

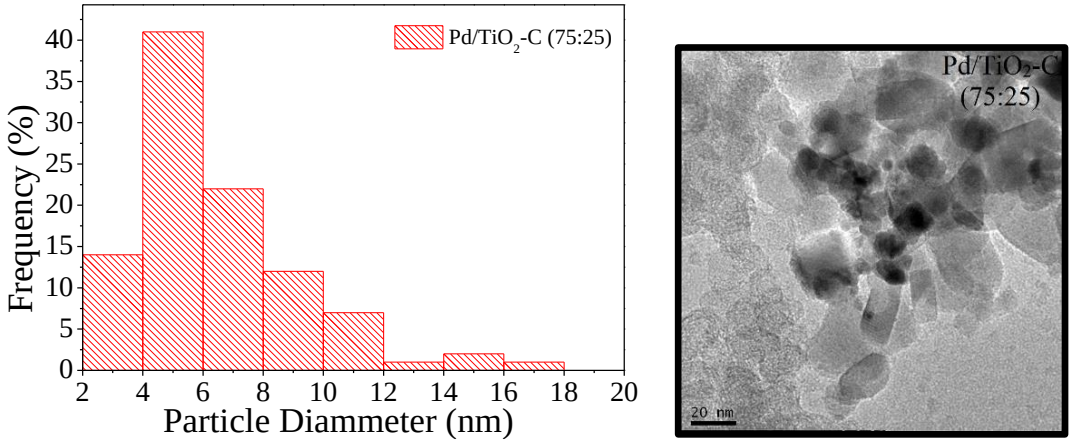

210

211

212 **Figure 1:** TEM images of the two batches of prepared materials: Pd/(C+TiO_2) where the
213 Pd nanoparticles were reduced in the physical mixture of carbon and TiO_2 and
214 Pd/TiO_2-C where the Pd nanoparticles were reduced firstly in TiO_2 and the carbon was
215 inserted after. Pd/C was also inserted for comparison.

216

217 Figure 2 presents XRD patterns for Pd/(C+TiO_2) and Pd/TiO_2-C batches. The
218 diffraction peaks at about 40.0º, 46.6º, 68.1º, and 82.1º are associated with (111), (200),
219 (220) and (311) planes, characteristic of the crystal face of Pd, as already observed before
220 [37] and according to JCPDF# 88-2335. From this figure, it is also possible to observe
221 peaks of the anatase phase of TiO_2 at 2θ = 25.3º, 37.8º, 48.0º, 53.9º, 55.1º, 62.7º, 68.8º,
222 70.3º and 75.0º and of rutile phase of TiO_2 at 2θ = 27.4º, 36.1º, 41.2º and 56.7º, as also

observed before [38]. The mean crystallite (estimated using the Scherrer equation) and average nanoparticle sizes are listed in Table 1. No shift was observed at the positions of the Pd diffraction peaks in the Pd/(C+TiO_2) and Pd/ TiO_2-C catalysts when compared to Pd/C, showing that the addition of TiO_2 does not affect the crystalline lattice of Pd [18].

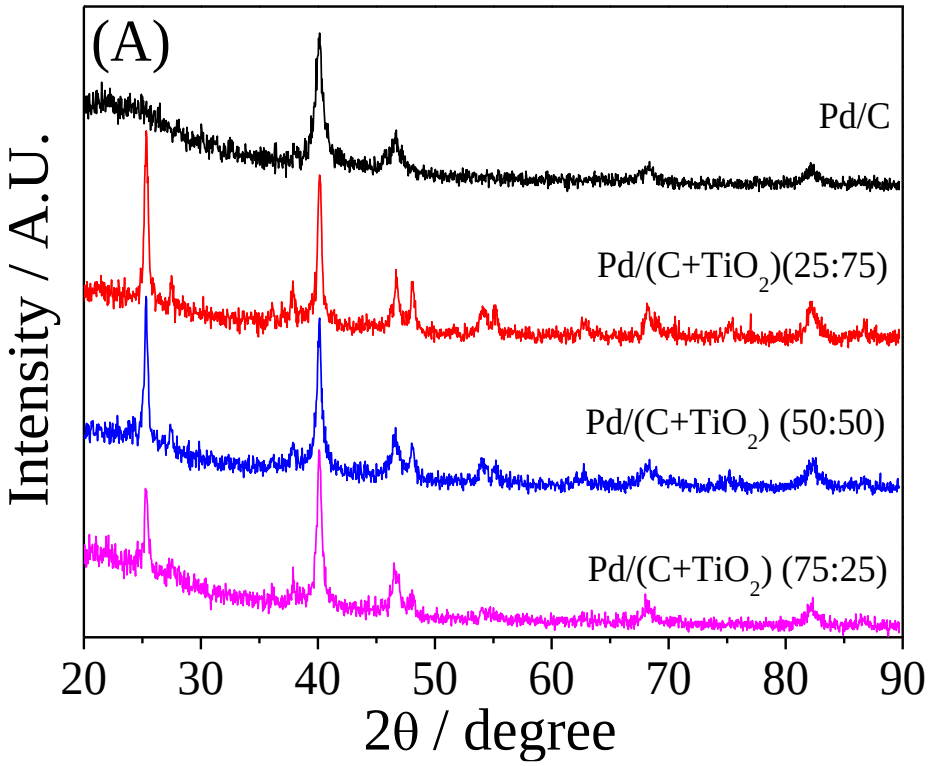

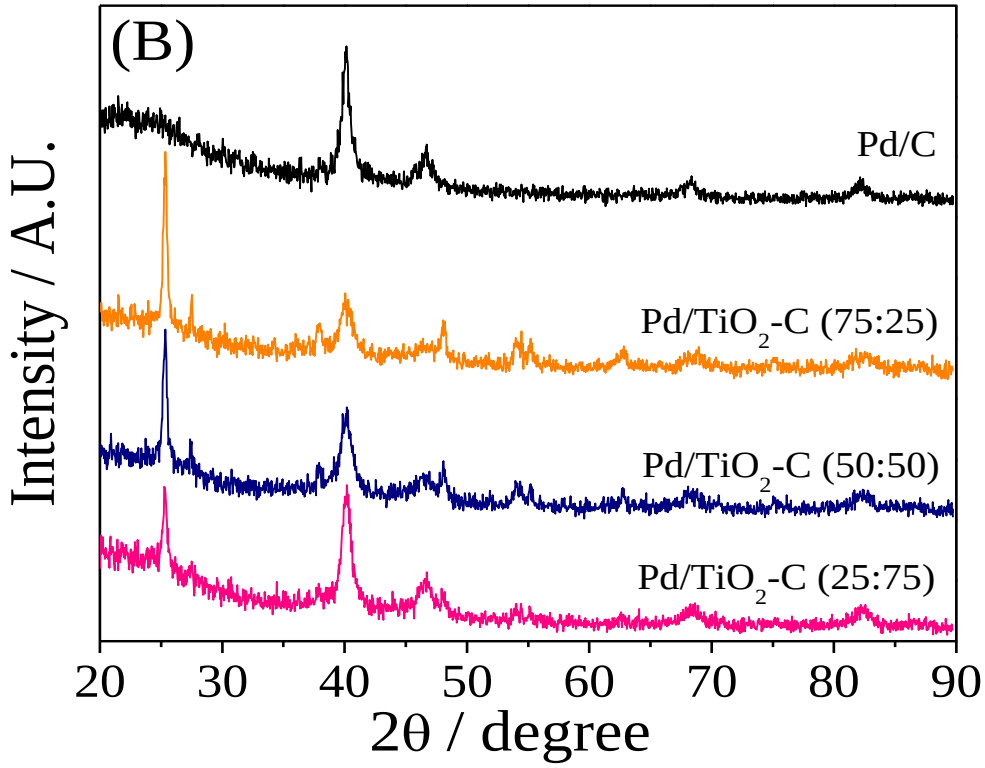

Figure 2: XRD patterns for: (A) Pd/(C+TiO_2) and (B) Pd/TiO_2-C electrocatalysts.

Table 1: Mean crystallite size obtained from XRD measurements and mean nanoparticle size obtained by TEM images.

Electrocatalysts	Mean crystallite size (XRD)	Mean nanoparticle size (TEM)
	nm	nm
Pd/C	6.0	3.7
Pd/(C+TiO_2) (25:75)	6.4	5.5
Pd/(C+TiO_2) (50:50)	7.5	7.9
Pd/(C+TiO_2) (75:25)	7.0	6.7
Pd/TiO_2-C (75:25)	3.6	5.4
Pd/TiO_2-C (50:50)	7.6	7.2
Pd/TiO_2-C (25:75)	4.9	6.4

238 3.2. Electrochemical Characterizations (half-cell)

239 EIS was employed to further study the electrochemical properties of the
240 electrocatalysts. Figure 3 presents the Nyquist (Figures 3A and B) and Bode
241 (Figures 3C-F) diagrams obtained. The spectra of all electrocatalysts correspond to a
242 simple Randles circuit, modified to incorporate the infinite diffusion related to Warburg
243 impedance ([R([RW]Q)]). The data of each circuit is available in Table 2, where R_S is the
244 solution resistance, R_{CT} is the charge transfer resistance, Y_0 is the admittance term, which
245 contains the diffusion coefficient information for the constant phase element (CPE) and
246 the Warburg impedance (W); and *n* is the exponential value of the CPE expression.

247 From these diagrams and fitted values, some behaviors can be inferred: the Bode
248 diagrams suggest hybrid capacitor and resistor behavior for this specific process. While
249 all phase value maximums are lower than $\pi/2°$, their presence at lower frequencies implies
250 that some charge effects are in motion during this process. These charge effects, along
251 with the relatively high *n* values, explain the loss of Nyquist plots' semi-circle definition.

252 The reduction of Pd in the C+TiO_2 mixture produced a material with a lower R_S
253 value at the 50:50 ratio when compared to 25:75 and 75:25. Also, the difference between
254 Pd/C and this material R_S is only ~9.0 Ω, implying a very small impact on the double
255 layer formation. This suggests that the addition of TiO_2 in the C support, by this method,
256 greatly affects its surface charge distribution when one of the components is in excess,
257 but not in the same proportions. Interestingly, the effect observed for the other method is
258 the opposite, as the direct deposition of Pd on TiO_2 and further addition of C at the same
259 proportion resulted in a significant increase in the R_S, while modestly increasing the R_S
260 in other distributions. As previously discussed, this could be the effect of the lower
261 electronic conductivity of TiO_2, and its inefficiency to produce active sites for PdNPs.
262 Among all electrocatalysts, both Pd/(C+TiO_2) (50:50) and Pd/TiO_2-C (50:50) presented

lower R_{CT} values (0.956 and 1.49 kΩ, respectively), a decrease of ~54 and ~29% when compared to Pd/C. This not only suggests that the addition of TiO_2 to the system is beneficial but also suggests that the predominant structure produced by the mixture method is considerably more conductive than the direct addition of Pd on TiO_2.

The *n* exponential value of the CPE expression is mathematically correlated to the roughness of the surface affecting the double electric layer formation, and it is close to 1.0 for completely smooth surfaces, such as pure metallic electrodes, with a decrease of this value as the roughness increases [39, 40]. The Pd/(C+TiO_2) (50:50) and Pd/TiO_2-C (75:25) presented a high *n* value when compared to all other electrocatalysts. This suggests that these materials, when cast on the electrodes, presented greater exposure or better distribution of the metals on the surface. This could be beneficial due to the increase in catalytic sites. Therefore, it could be expected that the Pd/(C+TiO_2) (50:50), Pd/TiO_2-C (75:25), and Pd/TiO_2-C (50:50) could present optimal performance in the half-cell analyses, due to their lower R_{CT} and/or greater metallic surface behavior.

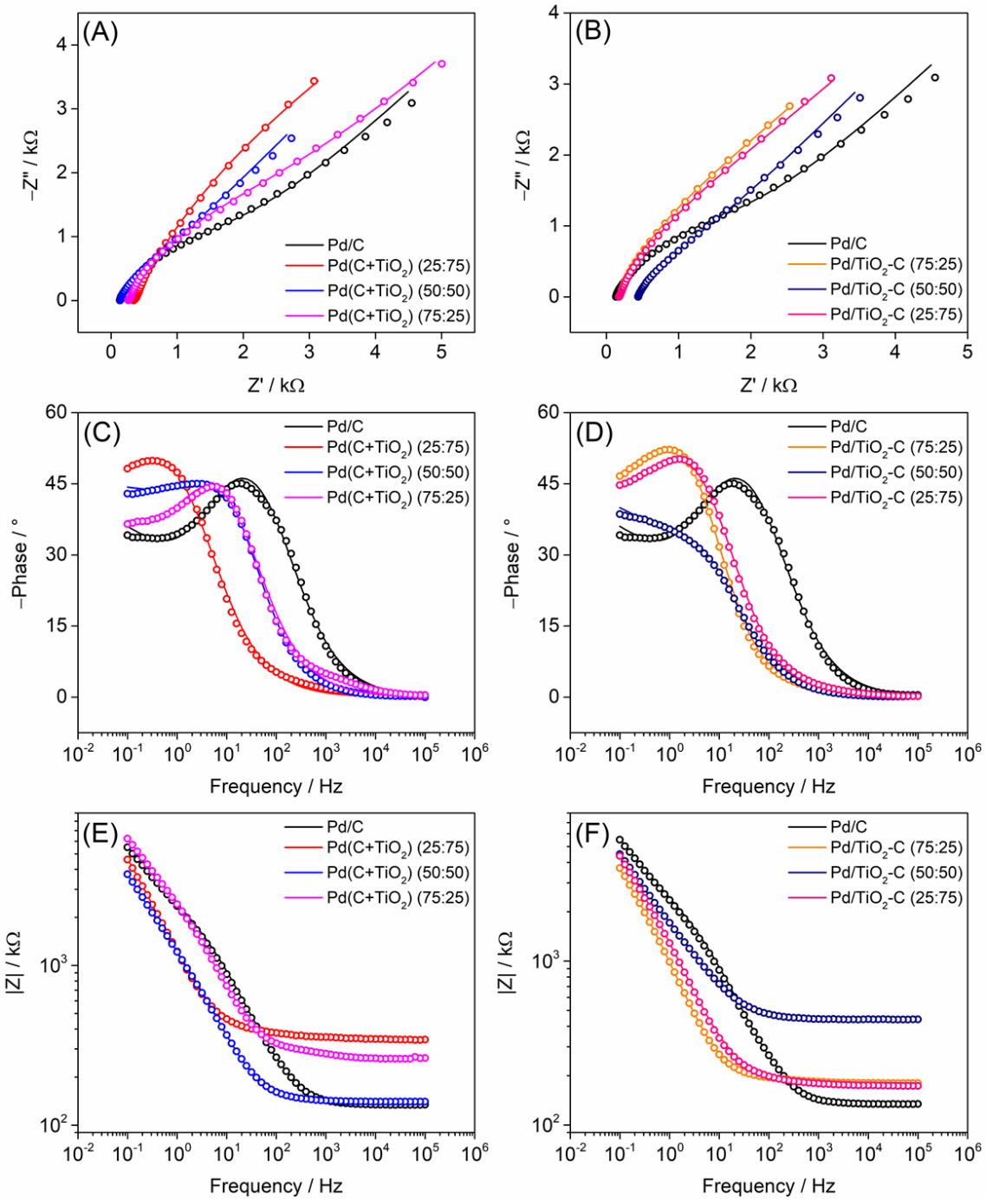

Figure 3. Nyquist diagrams of Pd/C and (A) Pd/(C+TiO_2) electrocatalysts; and (B) Pd/TiO_2-C electrocatalysts, in presence of 1.0 mmol L^{-1} $[Fe(CN_6)]^{3-/4-}$, in 0.1 mol L^{-1} KCl. *E* = 200 mV; Bode diagrams of (C and E) Pd/(C+TiO_2) and (D and F) Pd/TiO_2-C, in presence of 1.0 mmol L^{-1} $[Fe(CN_6)]^{3-/4-}$, in 0.1 mol L^{-1} KCl. *E* = 200 mV.

Table 2: Data obtained by [R([RW]Q)] equivalent circuit.

Electrocatalysts	R_S (Ω)	R_{CT} (kΩ)	CPE	Warburg impedance
Pd/C	131	2.090	Y_0 = 41.3 μS s^n n = 0.757	Y_0 = 273 μS $\sqrt{s}$
Pd/(C+TiO_2) (25:75)	351	10.30	Y_0 = 246 μS s^n n = 0.737	Y_0 = 305 μS $\sqrt{s}$
Pd/(C+TiO_2) (50:50)	140	0.9560	Y_0 = 108 μS s^n n = 0.815	Y_0 = 320 μS $\sqrt{s}$
Pd/(C+TiO_2) (75:25)	266	3.170	Y_0 = 68.1 μS s^n n = 0.761	Y_0 = 243 μS $\sqrt{s}$
Pd/TiO_2-C (75:25)	182	3.020	Y_0 = 220 μS s^n n = 0.816	Y_0 = 331 μS $\sqrt{s}$
Pd/TiO_2-C (50:50)	439	1.490	Y_0 = 104 μS s^n n = 0.745	Y_0 = 277 μS $\sqrt{s}$
Pd/TiO_2-C (25:75)	180	3.650	Y_0 = 174 μS s^n n = 0.765	Y_0 = 282 μS $\sqrt{s}$

Electrochemical properties and catalytic activities of the prepared electrocatalysts were evaluated using cyclic voltammetry. Figure 4 shows the cyclic voltammograms of both batches in 2.0 mol L^{-1} KOH. Pd/C was also inserted for comparison. From this figure it is possible to observe that the CVs are much similar, indicating that the introduction of TiO_2 has just little effect on the Pd profile [36]. It is also possible to observe peaks

associated with hydrogen desorption/adsorption around –0.7 and –0.8 V, respectively. In the forward scan and at ~ –0.3 V there is a peak associated with the formation of the palladium (II) oxide and, in the cathodic sweep, another peak at about –0.3 V, associated with the reduction of Pd oxide to Pd [41, 42]. For both batches, Pd/C showed the highest area, which could be attributed to the lower TiO_2 electric conductivity and surface area [32].

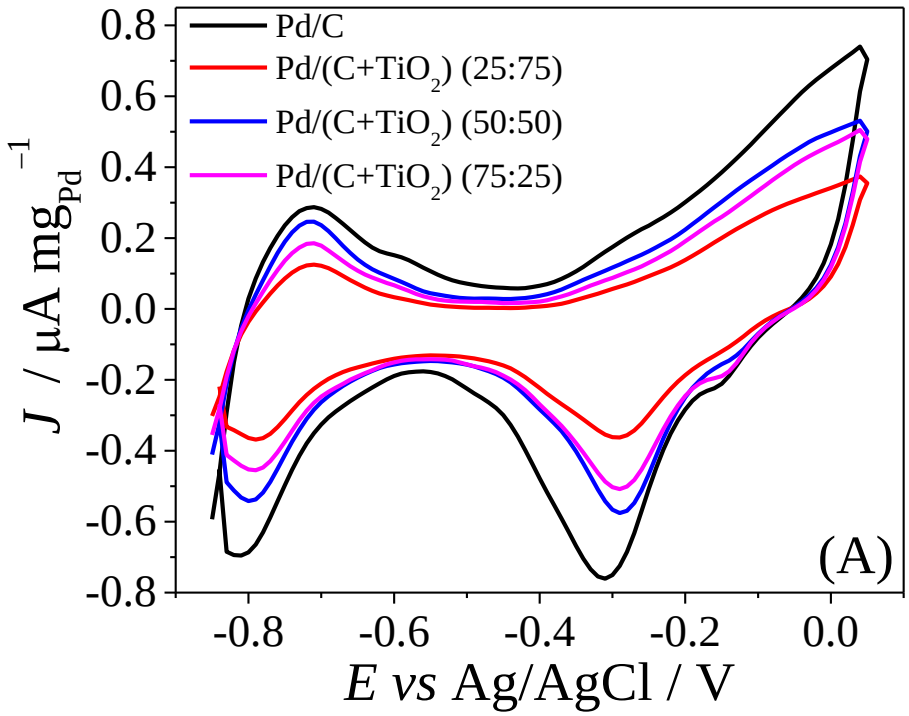

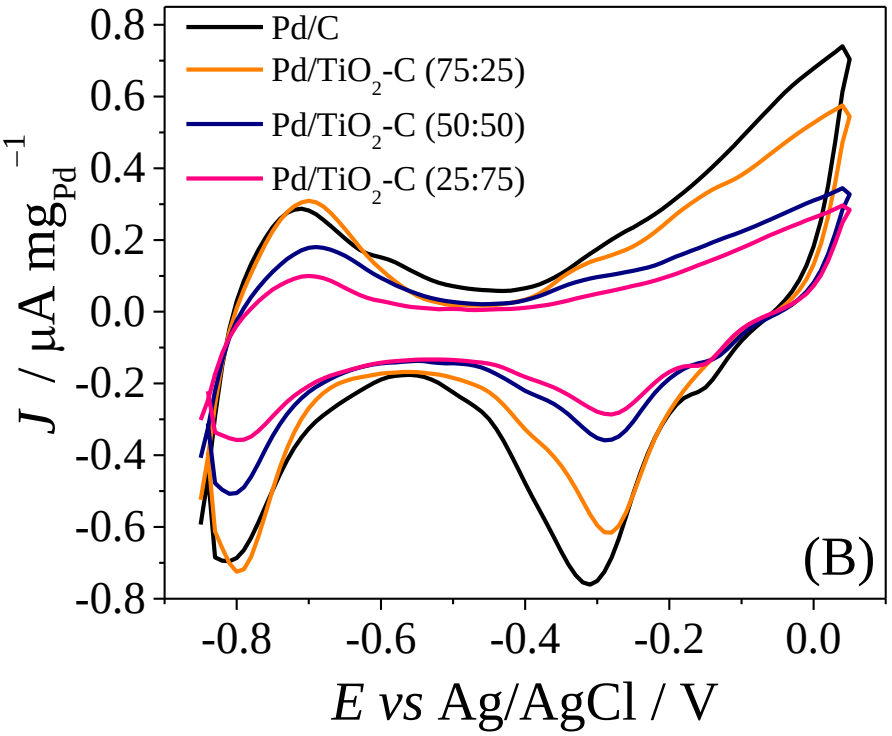

Figure 4: Cyclic voltammograms in 2.0 mol L^{-1} KOH at v = 10 mV s^{-1} for: (A) Pd/(C+TiO_2) and (B) Pd/TiO_2-C electrocatalysts.

Figure 5 presents the voltammetric pattern featuring the electro-oxidation of formate in alkaline media, which is characterized by two peaks. According to Noborikawa et al. [43], in the forward scan, there is a current increase until a point that the surface deactivates, which is caused by the oxide coverage. Besides, in the reverse scan, the surface oxides are reduced and the surface reactivates. Analyzing this figure, it is possible to affirm that all prepared materials are better than just Pd/C for formate electro-oxidation since they showed higher current densities when compared to Pd/C. However, among the materials in the study, Pd/(C+TiO_2) (50:50) and Pd/TiO_2-C (75:25) showed the highest currents toward formate oxidation, in agreement with the EIS analyses.

Many authors have indicated that oxide supports such as TiO_2 promote the oxidation of the poisoning intermediaries through the bifunctional mechanism while others attributed the higher catalytic activity in terms of metal reactivity variation due to

electronic interactions between noble metals and TiO_2 [44-46]. It has been observed that the adsorption of a water molecule on TiO_2 favors its dissociation, resulting in Ti-OH groups [24, 28] which could contribute to the enhanced activity of TiO_2 content catalysts.

In Antolini reviews [24], considering methanol oxidation on Pt-TiO_2, it was found that in presence of TiO_2, the electron transfer rate of methanol oxidation accelerated. Thus, the interaction between platinum active sites and the metal oxide could enhance the charge transfer at the interface but an excessive amount of TiO_2 could block some platinum active sites, decreasing the electrical conductivity of the catalyst. Moreover, the enhanced methanol oxidation reaction activity of Pt in the presence of TiO_2 has been attributed to both the bifunctional mechanism and the electronic effect.

Wang et al. [47] affirm that formate adsorbs on the Pd surface forms the stable intermediate species, HCO*O* (where the asterisks represent chemisorption to the surface). At room temperature, HCO*O* was slowly converted into HCOO* which is a reactive specie and thus, it rapidly formed hydride on the Pd surface and CO_2 was then released. According to some authors [48, 49], HCO*O* could act as a poisoning specie blocking the active Pd sites, and consequently, the catalytic activity toward formate oxidation could be increased by reducing the energy of the Pd-O bond, which in turn will lower the activation energy for the conversion of HCO*O* into HCOO* species.

According to Bai et al. [50] the formate oxidation reaction (FOR) on the Pd/C electrode undergoes a series of reactions in an alkaline medium, including $HCOO^-_{ad} \rightarrow H_{ad} + COO^-_{ad}$, $COO^-_{ad} \rightarrow CO_2 + e^-, H_{ad} + OH^-_{ad} \rightarrow H_2O + e^-$ and so on. Futhermore, they affirm that weak adsorption of $HCOO^-_{ad}$ facilitates the FOR and the FOR activity of catalysts also relates to OH^-_{ad} species, since the enhanced interaction between H_{ad} and OH^-_{ad} species also makes a special contribution to FOR activity enhancement. Choun et al. [51] report that H_{ad} species produced during the oxidation of

$HCOO^-$ is the important intermediate species since high coverage of H_{ad} inhibits the $HCOO^-$ adsorption onto Pd surfaces, causing slow oxidation kinetics of $HCOO^-$.

Hence, according to several studies [51-55], decreasing the chemisorption strength of adsorbed species by modifying the electronic structure of Pd can contribute to an enhancement in the catalytic activity. Therefore, the best results obtained using TiO_2 as support could be attributed to: the presence of Ti-OH surface groups, and/or the oxidation of the poisoning intermediaries through the bifunctional mechanism, and/or the electronic interactions between Pd and TiO_2.

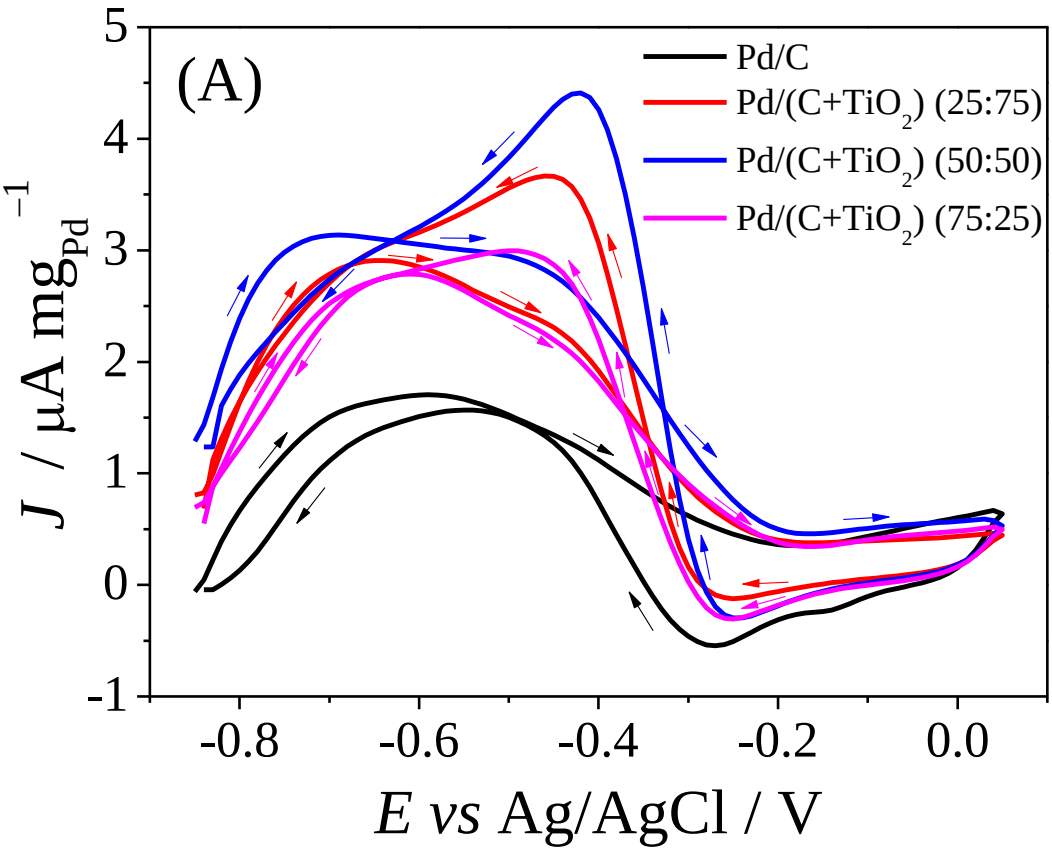

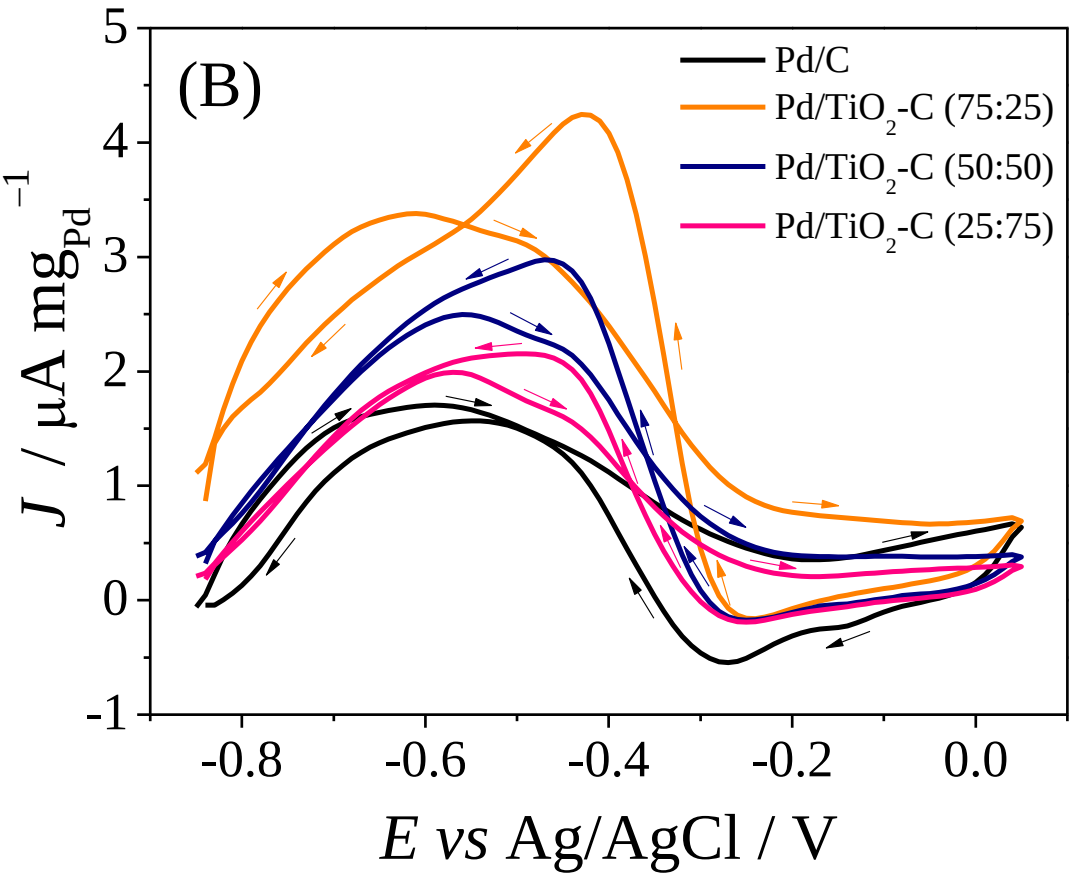

Figure 5: Cyclic voltammograms in 2.0 mol L^{-1} KOH + 0.02 mol L^{-1} potassium formate at v = 10 mV s^{-1} for: (A) Pd/(C+TiO_2) and (B) Pd/TiO_2-C electrocatalysts.

The stability of the electrocatalysts was evaluated through CA at a fixed potential, shown in Figure 6. As observed in the CV in presence of formate, all TiO_2 content electrocatalysts showed higher currents than Pd/C, indicating the activity of TiO_2 toward formate electro-oxidation. Moreover, the catalysts with TiO_2 content also showed the highest stability.

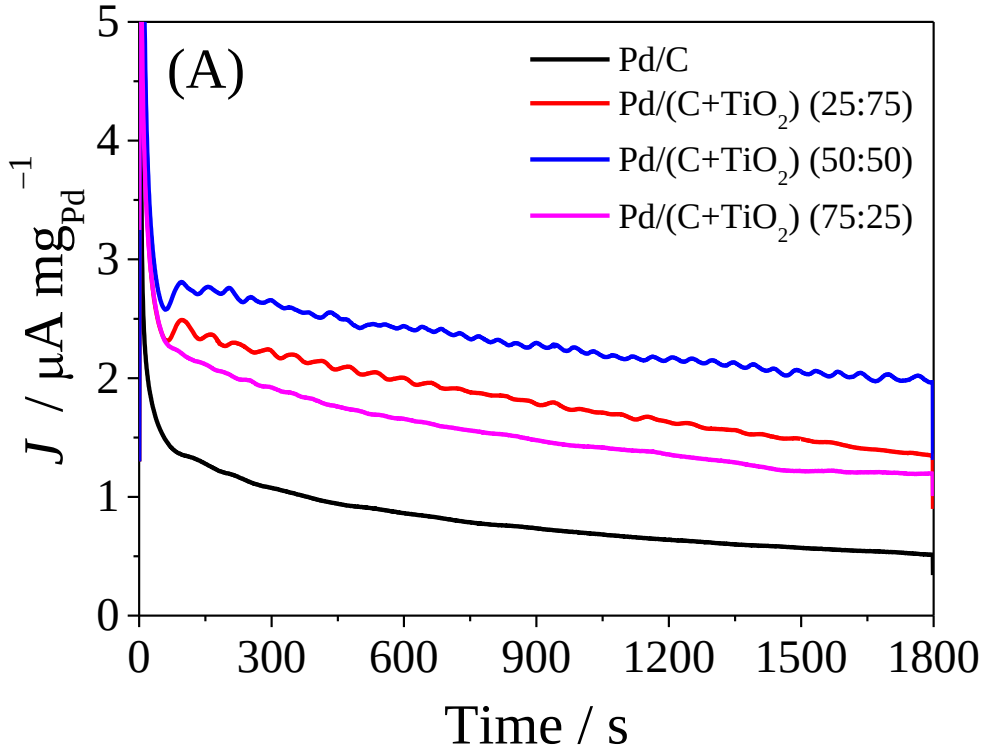

360

361

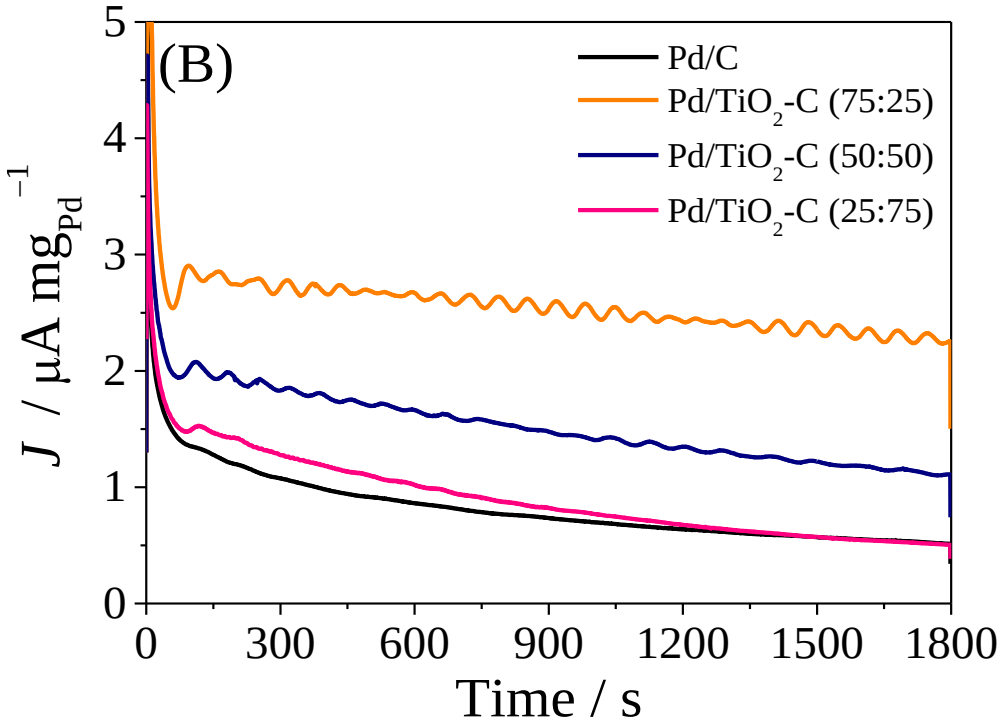

362

363 **Figure 6:** Chronoamperometric measurements at –0.55 V *vs* Ag/AgCl/KCl (3.0 mol L^{-1})

364 in 2.0 mol L^{-1} KOH + 0.02 mol L^{-1} potassium formate for: (A) Pd/(C+TiO_2) and (B)

365 Pd/TiO_2-C electrocatalysts.

366

367 Pd/TiO_2-C (75:25) showed higher current values compared to other prepared
368 electrocatalysts, however, Pd/TiO_2-C (25:75) showed similar performance in comparison
369 with Pd/C. All Pd/(C+TiO_2) showed higher current values compared with Pd/C, these
370 results confirmed that the activity of the prepared electrocatalysts is dependent on the
371 preparation method, but not entirely on the actual active area values at room temperature.
372

373 3.3. Fuel Cell Measurements (single cell)

374 Single-cell tests were performed to confirm the best activity of TiO_2 content
375 electrocatalysts in the direct formate fuel cell. Figure 7 shows the cell potential and power
376 density curves for all prepared electrocatalysts and the summarized results are available
377 in Table 3, showing open circuit potential (OCV) and maximum power density (MPD).

378 In contrast to the electrochemical measurements, all materials prepared to reduce
379 the Pd on the TiO_2 (Pd/TiO_2-C) showed maximum power densities lower than Pd/C,
380 showing that these materials were not efficient in a single-cell environment. Nevertheless,
381 the materials in which the Pd was reduced on the physical mixture of carbon and TiO_2,
382 Pd/(C+TiO_2), showed better power densities when compared to Pd/C, except the
383 Pd/(C+TiO_2) (25:75), in which the TiO_2 is in the major proportion.

384 According to Ahadi et al. [56], studying the conductivity in Pt/C electrocatalysts,
385 the only components of a catalytic layer (CL) that could conduct electrons are C and Pt
386 particles. On the other hand, the Pt particles have shown a small volume fraction when
387 compared to C particles. Thus, the electron conduction in CL should be determined by
388 the properties of the carbon phase. It is known that carbon supports are electronically
389 conductive and that carbon surface area provides the active sites for Pt nanoparticles [19,
390 57] while, due to the low d-band mobility, TiO_2 shows low electrical conductivity [58].

Matos et al. [26] studied the effect of TiO_2-C as support and evaluated also the effect of Pd supported on non-conductive support (Pd/SiO_2) and observed that the lack of the conductivity of the Pd/SiO_2 could be explained by the fact that Pd nanoparticles were fixed on non-conductive support. This information could explain the worst efficiency in single-cell experiments using Pd/TiO_2-C electrocatalysts, once in these materials, the PdNP were firstly reduced on TiO_2, which shows lower conductivity than carbon. As rutile and anatase are semiconductors, their conductivity may not be sufficient for a fuel cell application, which was not observed in CV results.

Besides, it is also known that the nature of the chosen support can modify the electronic structure of the active sites, leading to an improvement in its efficiency [57] and that the number of active sites, with ^{-}OH species adsorbed, is increased by the addition of TiO_2 and has particular importance in the fuel oxidation [49, 59, 60], what was observed with Pd/(C+TiO_2) electrocatalysts, except for the Pd/(C+TiO_2) (25:75), once, as already observed before [24], an excessive amount of TiO_2 could block some active sites, decreasing the electrical conductivity of the catalyst.

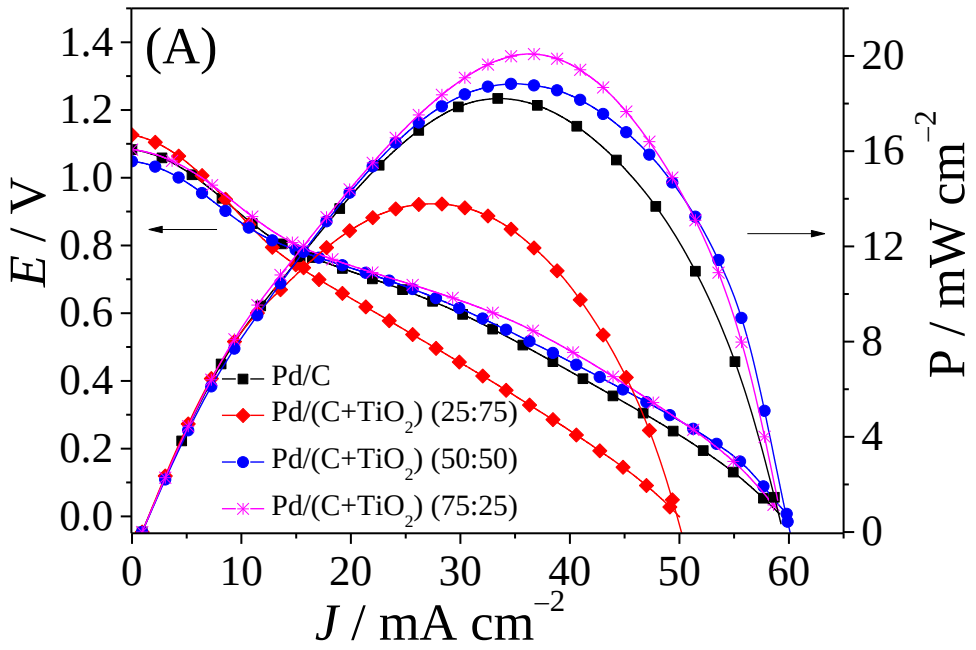

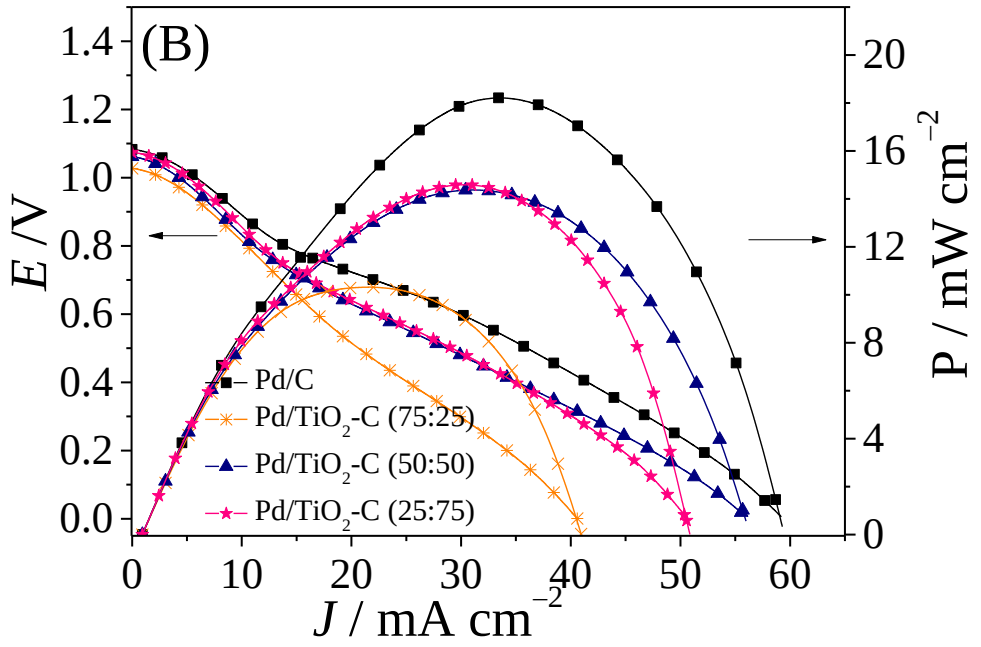

Figure 7: Power density and polarization curves of a 5 cm^2 direct formate fuel cell at 60 ºC using 1.0 mol L^{-1} HCOONa + 2.0 mol L^{-1} NaOH for: (A) Pd/(C+TiO_2) and (B) Pd/TiO_2-C electrocatalysts.

Table 3: Direct formate fuel cell results.

Electrocatalysts	MPD	Current Density	OCP
	mW cm^{-2}	mA cm^{-2}	V
Pd/C	18.2	59.2	1.08
Pd/(C+TiO_2) (25:75)	13.8	50.4	1.13
Pd/(C+TiO_2) (50:50)	18.8	60.1	1.05
Pd/(C+TiO_2) (75:25)	20.1	58.9	1.08
Pd/TiO_2-C (75:25)	10.3	40.9	1.03
Pd/TiO_2-C (50:50)	14.4	55.9	1.06
Pd/TiO_2-C (25:75)	14.6	50.7	1.07

4. Conclusions

Here, we report the effect of TiO_2 as support along with carbon, and also the synthesis strategies (by preparing two batches of electrocatalysts: Pd/(C+TiO_2) and Pd/TiO_2-C) toward formate electro-oxidation in alkaline media. The Pd/(C+TiO_2) electrocatalysts showed better results when compared to Pd/C, being the Pd/(C+TiO_2) (75:25) the best material achieved in fuel cell experiments which were justified by the higher content of carbon black which shows good electrical conductivity associated with small quantities of TiO_2 which works as co-catalyst on fuel oxidation, considering the bifunctional mechanism and/or metal reactivity variation due to electronic interactions between Pd and TiO_2.

Acknowledgments

The authors wish to thank Instituto de Pesquisa Energéticas e Nucleares by TEM measurements, Centro Nacional de Pesquisa em Energia e Materiais (CNPEM) and LNNano for XRD analysis, Conselho Nacional de Desenvolvimento Científico e Tecnológico – CNPq (407674/2016-0; 408430/2016-8; 169966/2017-8, 405546/2018-1; 103085/2019-0, and 403961/2021-1), Fundação de Amparo à Pesquisa do Estado de São Paulo – FAPESP (2017/21097-3, 2019/23342-0 and 2020/01050-5) and to the Coordenação de Aperfeiçoamento de Pessoal de Nível Superior - Brasil – CAPES,

Finance Code 001, 88887.504861/2020-00; for the financial support. The authors are also grateful to Evonik Degussa Brasil Ltda and Cabot Corporation for TiO_2 and Vulcan Carbon samples.

References

[1] J. Goldemberg, Energy Policy, (2006) https://doi.org/10.1016/j.enpol.2005.03.009.
[2] X.D. Wu, J.L. Guo, X. Ji, G.Q. Chen, Energy Policy (2019) https://doi.org/10.1016/j.enpol.2018.12.005.
[3] M.A. Hannan, M.S.H. Lipu, P.J. Ker, R.A. Begum, V.G. Agelidis, F. Blaabjerg, App. Energy (2019) https://doi.org/10.1016/j.apenergy.2019.113404.
[4] M. Child, O. Koskinen, L. Linnanen, C. Breyer, Renew. Sustain. Energy Rev. (2018) https://doi.org/10.1016/j.rser.2018.03.079.
[5] J.L. Aleixandre-Tudó, L. Castelló-Cogollos, J.L. Aleixandre, R. Aleixandre-Benavent, Renew. Energy (2019) https://doi.org/10.1016/j.renene.2019.02.079.
[6] A. Arshad, H.M. Ali, A. Habib, M.A. Bashir, M. Jabbal, Y. Yan, Therm. Sci. Eng. Prog. (2019) https://doi.org/10.1016/j.tsep.2018.12.008.
[7] R.A. Barreto, Econ. Model. (2018) https://doi.org/10.1016/j.econmod.2018.06.019.
[8] N. Edomah, Energy Rep. (2016) https://doi.org/10.1016/j.egyr.2016.01.004.
[9] M.V. Moreira, G.E. da Silva, Renew. Energy (2009) https://doi.org/10.1016/j.renene.2009.01.002.
[10] B.C. Ong, S.K. Kamarudin, S. Basri, Int. J. Hydrog. Energy (2017) https://doi.org/10.1016/j.ijhydene.2017.01.117.
[11] H.Q. Pham, T.T. Huynh, T.M. Pham, V.T.T. Ho, Int. J. Hydrog. Energy (2021) https://doi.org/10.1016/j.ijhydene.2020.08.278.
[12] D. Ye, Q. Lan, Q. Liao, Y. Yang, R. Chen, S. Wang, Z. Liu, X. Zhu, Carbon (2022) https://doi.org/10.1016/j.carbon.2022.02.053.
[13] O.C. Esan, X. Shi, Y. Dai, L. An, T.S. Zhao, Appl. Energy (2022) https://doi.org/10.1016/j.apenergy.2022.118677.
[14] E. Berretti, M.V. Pagliaro, A. Giaccherini, G. Montegrossi, F. Di Benedetto, G.O. Lepore, F. D'Acapito, F. Vizza, A. Lavacchi, Electrochim. Acta (2022) https://doi.org/10.1016/j.electacta.2022.140351.
[15] X. Sun, Y. Li, Int. J. Hydrog. Energy (2019) https://doi.org/10.1016/j.ijhydene.2019.01.240.
[16] A.O. Santos, J.C.M. Silva, R.M. Antoniassi, E.A. Ponzio, O.C. Alves, Int. J. Hydrog. Energy (2020) https://doi.org/10.1016/j.ijhydene.2020.08.165.
[17] S. Luo, Y. Wang, T.C. Kong, W. Pan, X. Zhao, D.Y.C. Leung, J. Power Sources (2021) https://doi.org/10.1016/j.jpowsour.2021.229526.
[18] A.M. Bartrom, J.L. Haan, J. Power Sources (2012) https://doi.org/10.1016/j.jpowsour.2012.04.032.
[19] R. Bock, H. Karoliussen, B.G. Pollet, M. Secanell, F. Seland, D. Stanier, O.S. Burheim, Int. J. Hydrog. Energy (2018) https://doi.org/10.1016/j.ijhydene.2018.10.221.
[20] L. Lan, J. Li, Y. Yang, L. Zhang, L. Zhang, Q. Fu, X. Zhu, Q. Liao, Carbon (2022) https://doi.org/10.1016/j.carbon.2021.12.071.
[21] L. An, R. Chen, J. Power Sources (2016) https://doi.org/10.1016/j.jpowsour.2016.04.082.

[22] J. Liu, H.J. Choi, L.-Y. Meng, J. Ind. Eng. Chem. (2018) https://doi.org/10.1016/j.jiec.2018.02.021.
[23] M.T. Anwar, X. Yan, S. Shen, N. Husnain, F. Zhu, L. Luo, J. Zhang, Int. J. Hydrog. Energy (2017) https://doi.org/10.1016/j.ijhydene.2017.10.152.
[24] E. Antolini, Appl. Catal. B: Environ. (2018) https://doi.org/10.1016/j.apcatb.2018.06.029.
[25] A.S. Bandarenka, M.T.M. Koper, J. Catal. (2013) https://doi.org/10.1016/j.jcat.2013.05.006.
[26] J. Matos, A. Borodzinski, A.M. Zychora, P. Kedzierzawski, B. Mierzwa, K. Juchniewicz, M. Mazurkiewicz, J.C. Hernández-Garrido, Appl. Catal. B: Environ. (2015) https://doi.org/10.1016/j.apcatb.2014.07.063.
[27] S.-Y. Huang, P. Ganesan, B.N. Popov, Appl. Catal. B: Environ. (2011) https://doi.org/10.1016/j.apcatb.2010.11.026.
[28] Y. Wang, J. Wang, G. Han, C. Du, Y. Sun, L. Du, M. An, G. Yin, Y. Gao, Y. Song, Appl. Surf. Sci. (2019) https://doi.org/10.1016/j.apsusc.2018.12.211.
[29] S. Samad, K.S. Loh, W.Y. Wong, T.K. Lee, J. Sunarso, S.T. Chong, W.R. Wan Daud, Int. J. Hydrog. Energy, (2018) https://doi.org/10.1016/j.ijhydene.2018.02.154.
[30] P. Sabatier, Ber. Dtch. Chem. Ges. (1911) https://doi.org/10.1002/cber.19110440303.
[31] A. Vittadini, A. Selloni, F.P. Rotzinger, M. Grätzel, Phys. Rev. Lett. (1998) 10.1103/PhysRevLett.81.2954.
[32] Q. Lv, M. Yin, X. Zhao, C. Li, C. Liu, W. Xing, J. Power Sources (2012) https://doi.org/10.1016/j.jpowsour.2012.06.051.
[33] S.G. da Silva, J.C.M. Silva, G.S. Buzzo, R.F.B. De Souza, E.V. Spinacé, A.O. Neto, M.H.M.T. Assumpção, Int. J. Hydrog. Energy (2014) https://doi.org/10.1016/j.ijhydene.2014.04.169.
[34] J.C.M. Silva, M.H.M.T. Assumpção, P. Hammer, A.O. Neto, E.V. Spinacé, E.A. Baranova, ChemElectroChem, (2017) 10.1002/celc.201600701.
[35] M.H.M.T. Assumpção, S.G. da Silva, R.F.B. De Souza, G.S. Buzzo, E.V. Spinacé, M.C. Santos, A.O. Neto, J.C.M. Silva, J. Power Sources (2014) https://doi.org/10.1016/j.jpowsour.2014.06.025.
[36] Y. Song, C. Wei, X. Zhang, X. Wei, X. Song, Z. Sun, Mat. Chem. Phys. (2015) https://doi.org/10.1016/j.matchemphys.2015.05.030.
[37] W.-L. Qu, Z.-B. Wang, Y. Gao, C. Deng, R.-H. Wang, L. Zhao, X.-L. Sui, Int. J. Hydrog. Energy (2018) https://doi.org/10.1016/j.ijhydene.2017.11.046.
[38] C. Wang, X. Cai, Y. Chen, Z. Cheng, X. Luo, S. Mo, L. Jia, P. Lin, Z. Yang, Chem. Eng. J. (2017) https://doi.org/10.1016/j.cej.2017.02.033.
[39] A. Lasia, Electrochemical impedance spectroscopy and its applications, in: Modern aspects of electrochemistry (Springer, 2002) pp. 143-248.
[40] A.R.C. Bredar, A.L. Chown, A.R. Burton, B.H. Farnum, ACS Appl. Energy Mat. (2020)
[41] Y.-H. Qin, Y. Zhuang, R.-L. Lv, T.-L. Wang, W.-G. Wang, C.-W. Wang, Electrochim. Acta (2015) https://doi.org/10.1016/j.electacta.2014.12.050.
[42] F. Zhang, D. Zhou, M. Zhou, J. Energy Chem. (2016) https://doi.org/10.1016/j.jechem.2015.10.013.
[43] J. Noborikawa, J. Lau, J. Ta, S. Hu, L. Scudiero, S. Derakhshan, S. Ha, J.L. Haan, Electrochim. Acta (2014) https://doi.org/10.1016/j.electacta.2014.04.188.
[44] A.E. Alvarez, A.N. Gravina, J.M. Sieben, P.V. Messina, M.M.E. Duarte, Mat. Sci. Eng.: B (2016) https://doi.org/10.1016/j.mseb.2016.05.017.

536 [45] C.-S. Chen, F.-M. Pan, Appl. Catal. B: Environ. (2009)
537 https://doi.org/10.1016/j.apcatb.2009.07.008.
538 [46] N. Rajalakshmi, N. Lakshmi, K.S. Dhathathreyan, Int. J. Hydrog. Energy (2008)
539 https://doi.org/10.1016/j.ijhydene.2008.09.032.
540 [47] W.J. Wang, S. Hwang, T. Kim, S. Ha, L. Scudiero, Electrochim. Acta (2021)
541 https://doi.org/10.1016/j.electacta.2021.138531.
542 [48] J.T. Gray, S.W. Kang, J.-I. Yang, N. Kruse, J.-S. McEwen, J.C. Park, S. Ha, Appl.
543 Catal. B: Environ. (2020) https://doi.org/10.1016/j.apcatb.2019.118478.
544 [49] J. Shim, C.-R. Lee, H.-K. Lee, J.-S. Lee, E.J. Cairns, J. Power Sources (2001)
545 https://doi.org/10.1016/S0378-7753(01)00817-5.
546 [50] J. Bai, Q. Xue, Y. Zhao, J.-X. Jiang, J.-H. Zeng, S.-B. Yin, Y. Chen, ACS Sustain.
547 Chem. Eng. (2019) 10.1021/acssuschemeng.8b06193.
548 [51] M. Choun, K. Ham, D. Shin, J.K. Lee, J. Lee, Catal. Today (2017)
549 https://doi.org/10.1016/j.cattod.2017.04.026.
550 [52] S. Hong, S. Chung, J. Park, J.P. Hwang, C.H. Lee, S. Uhm, S. Bong, J. Lee, ACS
551 Catal. (2021) 10.1021/acscatal.0c03555.
552 [53] J. Jiang, A. Wieckowski, Electrochem. Commun. (2012)
553 https://doi.org/10.1016/j.elecom.2012.02.017.
554 [54] T. Takamura, F. Mochimaru, Electrochim. Acta (1969)
555 https://doi.org/10.1016/0013-4686(69)80008-3.
556 [55] M. Choun, S. Hong, J. Lee, J. Electrochem. Soc. (2018) 10.1149/2.0341815jes.
557 [56] M. Ahadi, M. Tam, J. Stumper, M. Bahrami, Int. J. Hydrog. Energy (2019)
558 https://doi.org/10.1016/j.ijhydene.2018.12.016.
559 [57] G.R. Mirshekari, A.P. Shirvanian, J. Electroanal. Chem. (2019)
560 https://doi.org/10.1016/j.jelechem.2019.03.077.
561 [58] G.D. Bhowmick, M.T. Noori, I. Das, B. Neethu, M.M. Ghangrekar, A. Mitra, Int. J.
562 Hydrog. Energy (2018) https://doi.org/10.1016/j.ijhydene.2018.02.188.
563 [59] M. Kübler, T. Jurzinsky, D. Ziegenbalg, C. Cremers, J. Power Sources (2018)
564 https://doi.org/10.1016/j.jpowsour.2017.07.114.
565 [60] M. Choun, J. Lee, J. Energy Chem. (2016)
566 https://doi.org/10.1016/j.jechem.2016.04.008.
567